Pure appl. geophys. 157 (2000) 2323–2349
0033–4553/00/122323–27 $ 1.50 + 0.20/0

Pure and Applied Geophysics

Implications of a Statistical Physics Approach for Earthquake Hazard Assessment and Forecasting

V. G. KOSSOBOKOV,[1] V. I. KEILIS-BOROK,[1] D. L. TURCOTTE[2] and B. D. MALAMUD[2]

Abstract—There is accumulating evidence that distributed seismicity is a problem in statistical physics. Seismicity is taken to be a type example of self-organized criticality. This association has important implications regarding earthquake hazard assessment and forecasting. A characteristic of a thermodynamic system is that it exhibits a background noise that is self-organized. In the case of a dilute gas, this self-organization is the Maxwell–Boltzmann distribution of molecular velocities. In seismicity, it is the Gutenberg–Richter frequency-magnitude scaling; this scaling is fractal. Observations favor the hypothesis that smaller earthquakes in moderate-sized regions occur at rates that are only weakly dependent on time. Thus, the rate of occurrence of smaller earthquakes can be extrapolated to assess the hazard of larger earthquakes in a region. We obtain the rate of occurrence of earthquakes with $m > 4$ in $1° \times 1°$ areas from the NEIC catalog. Using only this data we produce global maps of the seismic hazard. Observations also favor the hypothesis that the stress level at which an earthquake occurs is a second-order critical point. As a critical point is approached, correlations extend over increasingly larger distances. In terms of seismicity, the approach to a critical point is associated with an increase in the rate of occurrence of intermediate-sized earthquakes prior to a large earthquake. This precursory activation has been shown to exhibit power-law scaling and to occur over a region about ten times larger than the rupture length of the large earthquake. Analyses of the spinoidal behavior associated with second-order critical points predict the power-law increase in seismic activity prior to a characteristic earthquake. This precursory activation provides the basis for intermediate-range earthquake forecasting.

Key words: Earthquake hazard assessment, self-organized critical behavior, inverse-cascade model, spinoidal behavior.

1. Introduction

Earthquakes constitute a major hazard in many of the earth's regions. The plate-tectonics hypothesis explains the concentration of earthquakes at plate boundaries, but significant numbers of earthquakes occur within plate interiors. The hypothesis of stick-slip behavior and elastic rebound explains the physics of

[1] International Institute of Earthquake Prediction Theory and Mathematical Geophysics, Russian Academy of Sciences, Warshavskoe sh. 79, kor. 2, Moscow 113556, Russia Federation. E-mails: volodya@mitp.ru and vkborok@mitp.ru

[2] Department of Geological Sciences, Cornell University, Ithaca, NY 14853-1504 U.S.A. E-mails: turcotte@geology.cornell.edu and bruce@malamud.com

earthquakes in a general way. Earthquakes occur on pre-existing faults and stick-slip events occur if the friction on the faults is velocity weakening. When the slip-event (earthquake) occurs, the elastic strains in the adjacent rock are relieved, generating seismic waves and heat. The laws of elasticity can be solved in a self-consistent manner to obtain periodic earthquake cycles.

However, earthquakes do not occur in periodic cycles. The earth's crust is extremely complex, and faults and earthquakes in a region occur on widely ranging scales. Considerable evidence exists that faults and earthquakes interact on a range of scales, from thousands of kilometers to millimeters or less. Evidence in support of this hypothesis stems from the universal validity of scaling relations. The most famous of these is the Gutenberg–Richter frequency-magnitude relation (GUTENBERG and RICHTER, 1954)

$$\log \dot{N}_{CE} = -bm + \log \dot{a} \tag{1}$$

where $\dot{N}_{CE}$ is the (cumulative) number of earthquakes with a magnitude greater than m occurring in a specified area and time, and b and $\dot{a}$ are constants. This relation is valid for earthquakes both regionally and globally. The constant b or "b-value" varies from region to region, but is generally in the range $0.8 < b < 1.2$ (FROHLICH and DAVIS, 1993). The constant $\dot{a}$ is a measure of the regional level of seismicity. There are a variety of measures for the magnitude, including local, body-wave, surface-wave, and moment magnitude (LAY and WALLACE, 1995). In general, for small-intensity earthquakes ($m < 5.5$), these different magnitude measures give approximately equivalent results.

Although the Gutenberg–Richter frequency-magnitude relation was originally developed as an empirical relation, we now recognize that it belongs to a broad range of natural phenomena that exhibit fractal scaling (TURCOTTE, 1989, 1997). For earthquakes, fractal scaling implies the validity of the relation

$$\dot{N}_{CE} = C A_E^{-\alpha} \tag{2}$$

where $\dot{N}_{CE}$ is the (cumulative) number of earthquakes with rupture area greater than A_E occurring in a specified area and time; C and α are constants with $D = 2\alpha$ the fractal dimension. AKI (1981) showed that (1) and (2) are entirely equivalent with

$$\alpha = b = D/2. \tag{3}$$

Thus, the universal applicability of the Gutenberg–Richter relation implies universal fractal behavior of earthquakes. Other natural phenomena that satisfy fractal scaling relations include landslides (PELLETIER *et al.*, 1997) and forest fires (MALAMUD *et al.*, 1998).

The fractal behavior of seismicity can be associated with chaotic behavior and self-organized criticality (TURCOTTE, 1999a). This association is illustrated by the behavior of slider-block models. These models are considered analogs for the

behavior of faults in the earth's crust. The simplest example is a single slider block of mass m pulled over a surface by a spring attached to a constant-velocity driver plate. The interaction of the block with the surface is controlled by friction. Many friction laws have been proposed; the simplest is the static-dynamic friction law. If the block is stationary, the static frictional force is F_s, if the block is slipping the dynamical frictional force is F_d. If $F_s > F_d$ stick-slip behavior is obtained, the motion of the block comprises periodic slip events.

The behavior of a pair of slider blocks pulled over a surface and connected by a connector spring was studied in detail by HUANG and TURCOTTE (1990). The equations of motion for the two blocks were solved simultaneously. Solutions were governed by two parameters: the stiffness of the system, k_c/k_p (k_c spring constant of the connector spring and k_p the spring constant of the puller springs) and the ratio of static to dynamic friction, F_s/F_d. For some values of these parameters, deterministic chaos was found. Chaotic behavior requires some asymmetry in the problem, i.e., $F_{s1} \neq F_{s2}$. The period doubling route to chaos was observed with positive values of the Lyapunov exponent in the chaotic regions. The behavior of the pair of slider blocks is very similar to the behavior of the logistic map (MAY, 1976).

The chaotic behavior of the low-dimensional Lorenz equations (LORENZ, 1963) is now accepted as evidence that the behavior of the atmosphere and oceans is chaotic. Similarly, the chaotic behavior of a pair of slider blocks is evidence that earthquakes exhibit chaotic behavior. It is instructive to make comparisons between the behavior of the earth's atmosphere and the behavior of the earth's crust. Massive numerical simulations are routinely used to forecast the weather. In many cases, they are quite accurate on time scales of 24 to 48 hours, however on the scale of weeks, they are of little value. The motions of the storm systems are relatively stable, considering the complexity involved. In many cases, the paths of major storms such as hurricanes can be predicted with considerable accuracy, but in other cases there are major uncertainties.

What about the earth's crust? Forecasting or predicting an earthquake is quite different than forecasting the path and intensity of a hurricane (TURCOTTE, 1991). The hurricane exists but the earthquake does not exist until it happens. GELLER *et al.* (1997) have argued, based on the chaotic behavior of the earth's crust, that "earthquakes cannot be predicted." This is certainly true in the sense that the exact time of occurrence of an earthquake cannot be predicted. However, this is also true of hurricanes, the exact path of a hurricane cannot be predicted. Nevertheless, a probabilistic forecast of hurricane paths with a most probable path are routinely made, and their use is of great value in terms of requiring evacuations and in other preparations. An essential question concerning earthquakes is whether similar useful probabilistic forecasts can be made. In fact, this is already being done in terms of hazard assessments. The rate of occurrence of small earthquakes is extrapolated to estimate the rate of occurrence of larger earthquakes.

The applicability of power-law (fractal) scaling to earthquakes can be justified in terms of scale-invariance; the power-law distribution is the only distribution that does not require a characteristic length scale. However, there is accumulating evidence that a more fundamental reason exists. In the past ten years, a variety of numerical models have been found to exhibit a universal behavior that has been called self-organized criticality. In self-organized criticality the ''input'' to a complex system is slow and steady; whereas the output is a series of events or ''avalanches'' that follow power-law (fractal) frequency-size statistics. Regional seismicity is often taken as a naturally occurring example of self-organized criticality. The input is the slow and steady motion of the tectonic plates and the output is the earthquakes.

The concept of self-organized criticality (TURCOTTE, 1999b) evolved from the ''sandpile'' model proposed by BAK *et al.* (1988). In this model there is a square grid of boxes and at each time step a particle is dropped into a randomly selected box. When a box accumulates four particles, they are redistributed to the four adjacent boxes, or in the case of edge boxes, they are lost from the grid. Since only nearest-neighbor boxes are involved in a redistribution, this is a cellular-automata model. Redistributions can lead to further instabilities and avalanches of particles in which many particles may be lost from the edges of the grid. The input is the steady-state addition of particles. A measure of the state of the system is the average number of particles in the boxes. This ''density'' fluctuates about a quasi-equilibrium value. Each of the multiple redistributions during a time step contributes to the size of the model ''avalanche.'' One measure of the size of a model avalanche is given by the number of particles lost from the grid during each sequence of redistributions; an alternative measure is given by the number of boxes that participate in the redistributions.

This model is called a ''sandpile'' model because of the resemblance to an actual sandpile on a table. The randomly dropped particles in the model are analogous to the addition of particles to an actual sandpile; the model avalanches are analogous to sand avalanches down the sides of the sandpile. In some cases, the sand avalanches lead to the loss of particles off the table. Extensive numerical studies of the ''sandpile'' model were carried out by KADANOFF *et al.* (1989). They found that the noncumulative frequency-size distribution of avalanches satisfies (2) with $\alpha \approx 1.0$.

A second example of ''self-organized criticality'' is the behavior of large arrays of slider blocks. The slider block model with a pair of slider blocks considered above can be extended to include large numbers of slider blocks. Multiple slider-block simulations were first considered by BURRIDGE and KNOPOFF (1967). OTSUKA (1972) considered a two-dimensional array of slider blocks and obtained power-law distributions for the size of slip events.

CARLSON and LANGER (1989) considered long linear arrays of slider blocks with each block connected by springs to the two neighboring blocks and to a

constant-velocity driver. They used a velocity-weakening friction law and considered up to 400 blocks. Slip events involving numerous blocks were observed, the motions of all blocks involved in a slip event were coupled, and the applicable equations of motion had to be solved simultaneously. Because of the strong similarities, these are often known as molecular-dynamic simulations. Although the system is completely deterministic, the behavior was apparently chaotic. Frequency-size statistics were obtained for slip events. The events fell into two groups. In the first group, smaller events obeyed a power-law (fractal) relationship with a slope near unity. In the second group, there was an anomalously large number of large events that included all the slider blocks. The observed behavior was characteristic of self-organized criticality. The motion of the driver plate is the steady input. The slip events are the avalanches with a fractal distribution.

NAKANISHI (1991) studied multiple slider-block models using the cellular-automata approach. A linear array of slider blocks was considered but only one block was allowed to move in a slip event. The slip of one block could lead to the instability of either or both of the adjacent blocks, which would then be allowed to slip in a subsequent step or steps, until all blocks were again stable. BROWN *et al.* (1991) proposed a modification of this model involving a two-dimensional array of blocks. The use of the cellular-automata approach greatly reduces the complexity of the calculations and the results using the two approaches are generally very similar. A wide variety of slider-block models have been proposed and studied; these have been reviewed by CARLSON *et al.* (1994) and TURCOTTE (1997).

The standard multiple slider-block model consists of a square array of slider blocks as illustrated in Figure 1. Each block with mass m is attached to the driver plate with a driver spring, spring constant k_p. Adjacent blocks are attached to each other with connector springs, spring constant k_c. A block remains stationary as long as the net force on the block is less than the static resisting force, F_s. If the static frictional force is greater than the dynamic frictional force, $F_s > F_d$, stick-slip behavior is observed. In order to carry out a simulation it is necessary to specify the stiffness, k_c/k_p, the friction, F_s/F_d, and the area of the square array.

HUANG *et al.* (1992) carried out numerous simulations on a square array of blocks using stick-slip friction and a cellular-automata approach. Their noncumulative frequency-area statistics for model slip events are given in Figure 2. The number of slip events per time step with area A_e, N_e/N_0, is given as a function of A_e. Results are given for a stiffness $k_c/k_p = 30$, friction $F_s/F_d = 1.5$, and four grid sizes, 20×20, 30×30, 40×40, and 50×50. There is good agreement with the power-law relation (2) taking $\alpha \approx 1$. For stiff systems, k_c/k_p large, the entire grid of slider blocks is strongly correlated and large slip events including all blocks occur regularly. These are the peaks for $A_e = 400$, 900, and 1600, illustrated in Figure 2. For soft systems, k_c/k_p relatively small, no large events occur.

There are strong similarities between the behavior of the sandpile model and the slider-block model. In both cases, smaller slip events have a noncumulative power-

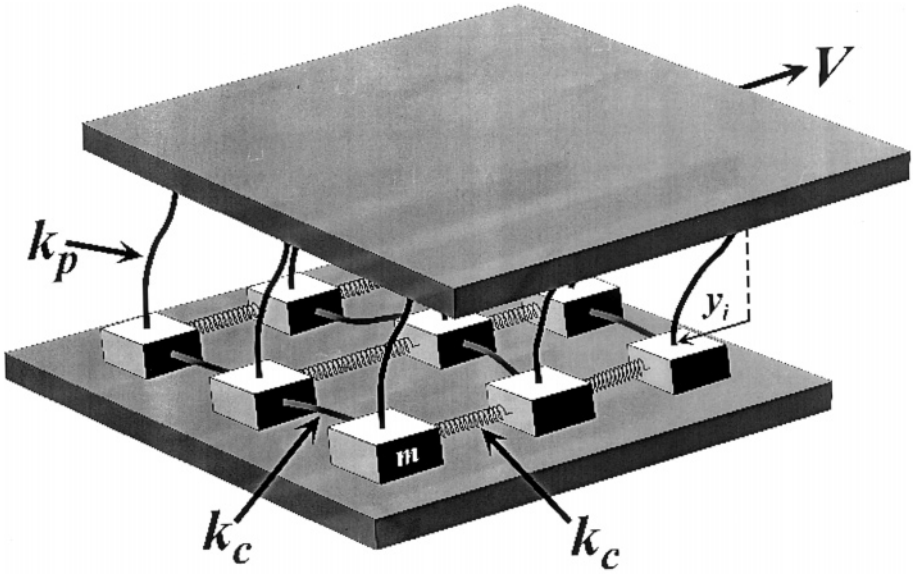

Figure 1
Illustration of the two-dimensional slider-block model. An array of blocks, each with mass m, is pulled across a surface by a driver plate at a constant velocity, V. Each block is coupled to the adjacent blocks with either leaf or coil springs (spring constant k_c), and to the driver plate with leaf springs (spring constant k_p).

law frequency-area distribution with a slope near unity. Whereas the sandpile model is stochastic in the selection of boxes, the slider-block model is fully deterministic. The slider-block model provides a bridge between chaotic behavior (two slider blocks) and self-organized critical behavior (large numbers of slider blocks). Adjacent solutions for the chaotic behavior of a pair of slider blocks have an exponential divergence. Adjacent solutions for large numbers of slider blocks have a power-law divergence.

The power-law distribution of avalanches in the sandpile and slider-block models can be explained in terms of an inverse cascade (TURCOTTE *et al.*, 1999). A metastable cluster is a group of boxes in the sandpile model or a group of slider blocks in the slider-block model over which an avalanche will spread once it is initiated. The inverse cascade is the coalescence of smaller metastable regions to form larger metastable regions. This coalescence gives a power-law distribution of metastable cluster sizes. Avalanches sample this distribution and thus also have a power-law distribution of sizes. However, significant numbers of metastable clusters are lost only from the largest cluster sizes, and these losses terminate the cascade and the region of power-law scaling.

Since the concept of self-organized criticality was first introduced, earthquakes have been identified as an example of this phenomenon in nature (BAK and TANG,

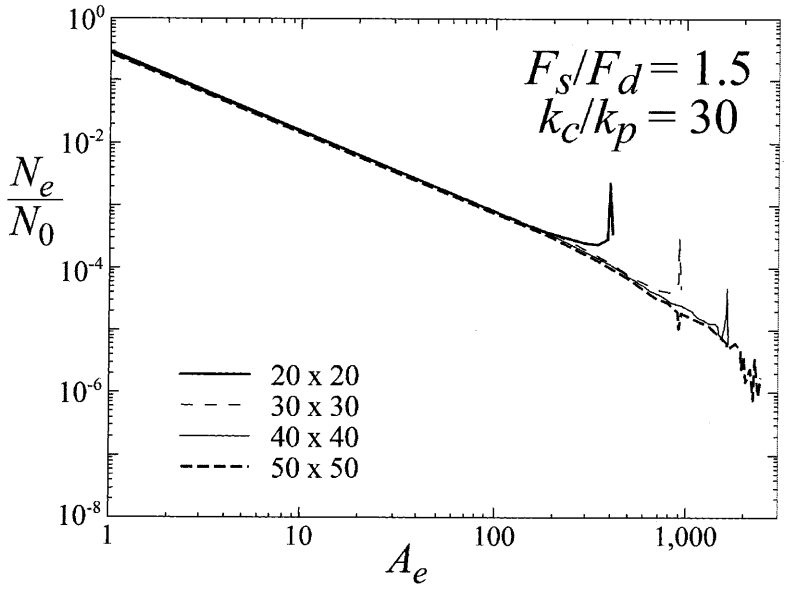

Figure 2
Results for a two-dimensional slider-block model with multiple blocks (HUANG *et al.*, 1992). The ratio of the number of slip events, N_e, with area A_e, to the total number of slip events N_0, is plotted against A_e the number of blocks involved in an event (HUANG *et al.*, 1992). Results are given for systems with stiffness $k_c/k_p = 30$, friction $F_s/F_d = 1.5$, and grid sizes 20×20, 30×30, 40×40, and 50×50. The peaks at $A_e = 400$, 900, and 1600, correspond to catastrophic slip events involving the entire system.

1989). These authors also pointed out the similarity in slopes between self-organized critical behavior and earthquakes. However, since the model data are noncumulative, the agreement with the cumulative earthquake data must be considered fortuitous. The power-law exponents are significantly higher for the application than for the model.

There is also accumulating observational evidence that the occurrence of an earthquake is equivalent to a critical point. The evidence for precursory seismic activation prior to an earthquake will be discussed in Section 3 of this paper. This activation is the primary basis for the intermediate-range earthquake prediction algorithms developed by Keilis-Borok and his associates (KEILIS-BOROK, 1990, 1996; KEILIS-BOROK and KOSSOBOKOV, 1990; KEILIS-BOROK and ROTWAIN, 1996; KNOPOFF *et al.*, 1996; KOSSOBOKOV *et al.*, 1999). This activation is associated with the approach of the "tuning parameter," the regional stress, to the critical value that will result in an earthquake. As the critical point is approached, the correlation length increases. For an earthquake, the correlation length is the size of the region over which precursory seismic activation occurs. BOWMAN *et al.* (1998) give observational evidence that the correlation length is about ten times the length of the rupture zone. It appears reasonable to hypothesize that seismicity in the earth's

crust is a thermodynamic system. Small earthquakes represent a background noise that is independent of time and does correlate with the ''seismic cycle.'' The rate of occurrence of small earthquakes is proportional to the rate of increase of the regional stress (the tuning parameter), and this is proportional to the rate of occurrence of the larger earthquakes. This hypothesis is the basis of our approach to probabilistic seismic hazard assessment given in the next section.

2. Hazard Assessment

The validity of the Gutenberg–Richter frequency-magnitude relation (1) for regional seismicity has been recognized for approximately 50 years. The use of this relation to extrapolate the rate of occurrence of small earthquakes to larger earthquakes (CORNELL, 1968) has been routinely incorporated into many regional seismic hazard assessments in a number of developed countries. Probably the best-documented probabilistic seismic hazard assessment was developed for the eastern United States by the Lawrence Livermore National Laboratory under a contract from the U.S. Nuclear Regulatory Commission. The documentation runs to eight volumes with some 3000 pages (BERNREUTER *et al.*, 1989). The objective was to assess the seismic hazard for nuclear power plant operation in the eastern United States.

In their study, the use of the Gutenberg–Richter frequency-magnitude relation (1) was an essential feature of the hazard assessment. However, a standard approach to its use could not be agreed upon. As a first step, the eastern United States was divided into 35 zones based on geological considerations. ''Expert opinion'' was then used to obtain values for the parameters $\dot{a}$ and b in (1). For each of the 35 zones, eleven ''experts'' were asked to provide their ''preferred'' values of these parameters based on their own estimates. The different experts used different selections of earthquakes, different corrections to magnitudes (for instrumental and historic events) and different treatments of aftershocks. As an example, for Zone 1 (New England), in the equation $\log N_{CE} = -bm + a$, values of a ranged from 2.68 to 4.39 and the values of b ranged from 0.60 to 1.15. Note that a in their equation is for the entire period whereas our $\log \dot{a}$ in (1) is per year. The report concluded that the frequency of occurrence predictions in a region could have errors as large as factors of 40–100.

The United States Geological Survey prepares seismic hazard maps for the United States. The most recent version (FRANKEL *et al.*, 1996) systematically utilized the Gutenberg–Richter relation (1). Details of the approach for the eastern United States have been given by FRANKEL (1995). First, the region was divided into 11 km by 11 km cells. Then the number of earthquakes N_i in each cell i with magnitudes greater than a given m was determined. Thereafter the grid of N_i values was spatially smoothed using a Gaussian function with a correlation distance c. A

map of smoothed 10^a values was prepared (FRANKEL, 1995, Fig. 4) taking $m = 3$ (1924–1991) and $c = 50$ km. The optimal c-value of about 50 km was found through trial and error.

In this paper, we propose a systematic approach to the use of the Gutenberg–Richter relation (1) to estimate the seismic hazard globally, using a method very similar to the one just discussed (FRANKEL, 1995). In particular, we must choose an earthquake catalog and a lower-magnitude cutoff that gives reasonable completeness for a specified period of time. Then we must also choose an area over which to average the observed seismicity. Finally, we directly use the Gutenberg–Richter relation (1) to extrapolate the occurrence of small earthquakes in order to assess the hazard of larger earthquakes.

Before discussing the global approach we consider two specific examples of the application of the Gutenberg–Richter relation to earthquake hazard assessment. We consider the regional seismicity in two localities, Southern California and the New Madrid seismic zone.

The cumulative frequency-magnitude distribution of seismicity in Southern California is given in Figure 3. The data, from the Southern California Seismographic Network (SCSN CATALOG, 1995) are for the period 1932–1994. The

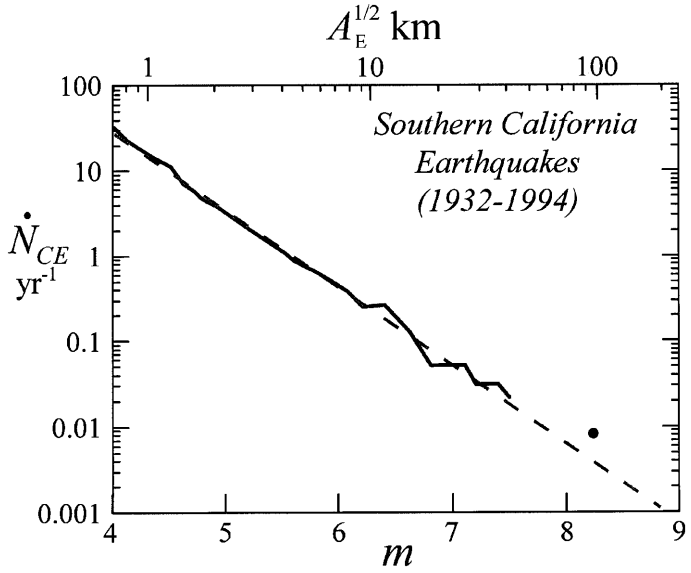

Figure 3
Cumulative number of earthquakes per year, $\dot{N}_{CE}$, occurring in Southern California with magnitudes greater than m as a function of m. Also given is the square-root of the equivalent rupture area. The solid line is for the time period 1932–1994, with data obtained from the SCSN CATALOG (1995). The straight dashed line is the Gutenberg–Richter relation (1) with $b = 0.92$ and $\dot{a} = 1.4 \times 10^5$ yr^{-1}. The solid circle is the observed occurrence rate of great earthquakes in Southern California (SIEH, 1978; SIEH *et al.*, 1989).

catalog contains a variety of magnitude measures. The cumulative number of earthquakes per year, $\dot{N}_{CE}$, with magnitudes greater than m, are given as a function of m. Over the range $4.0 < m < 7.5$, the data in Figure 3 are in excellent agreement with the straight dashed line, obtained by taking the Gutenberg–Richter relation (1) with $b = 0.92$ and $\dot{a} = 1.4 \times 10^5$ yr^{-1}.

Also included in Figure 3 is a solid circle representing the value associated with great earthquakes on the southern section of the San Andreas Fault. Dates for ten large earthquakes on this fault section have been obtained from radiocarbon dating of liquefaction features (SIEH, 1978). The mean repeat time is 132 years, giving $\dot{N}_{CE} = 0.0076$ yr^{-1}. SIEH *et al.* (1989) estimated that the last great earthquake, in 1857, had a magnitude $m = 8.25$. Taking these values for $\dot{N}_{CE}$ and m, we obtain the solid circle in Figure 3. An extrapolation of the Gutenberg–Richter statistics (the dashed line in Fig. 3) appears to make a reasonable prediction of great earthquakes on this section of the San Andreas Fault. It must be noted that the extrapolation of the levels of regional seismicity to regional "characteristic" earthquakes is controversial (DAVISON and SCHOLZ, 1985; PACHECO *et al.*, 1992; SCHOLZ, 1997). But, even without this extrapolation to "characteristic" earthquakes, this assessment provides valuable information on the regional seismic hazard for moderate-sized earthquakes.

An essential question concerning the extrapolation of background seismicity to estimate the seismic hazard, is the time dependence of the background seismicity. If the background seismicity increased systematically during an earthquake cycle, this increase could be used for earthquake prediction. There is no evidence for such a systematic increase.

The second question is the statistical temporal variability of regional seismicity. To address this question, we consider the time dependence of the background seismicity in Southern California. The frequency-magnitude distributions of the regional seismicity in Southern California on a yearly basis are plotted in Figure 4 using data obtained from the SCSN CATALOG (1995). Again, this catalog contains a variety of magnitude measures. For each individual year between 1980–1994, the cumulative number of earthquakes $\dot{N}_{CE}$ with magnitudes greater than m is plotted as a function of m. The period 1980–1994 taken together results in the Gutenberg–Richter power-law relation (1) with $b = 1.05$ and $\dot{a} = 2.06 \times 10^5$ yr^{-1}, shown as the solid straight lines in Figures 4a–c. In Figure 4, there is generally good agreement between each individual year's data and the Gutenberg–Richter relation (solid straight line) for the period 1980–1994. The exceptions can be attributed to the aftershock sequences of the 1987 Whittier, 1992 Landers, and 1994 Northridge earthquakes.

With aftershocks removed, the background seismicity in Southern California illustrated in Figure 4 is nearly uniform from year to year, and is not a function of time. Small earthquakes behave like a thermal background noise. This is observational evidence that the earth's crust is continuously on the brink of failure

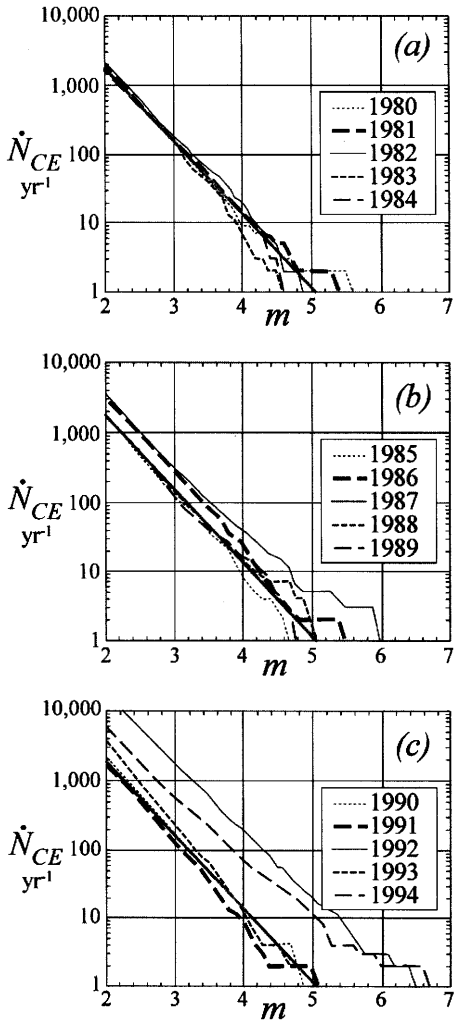

Figure 4

Cumulative number of earthquakes per year, $\dot{N}_{CE}$, occurring in Southern California with magnitudes greater than m as a function of m. Fifteen individual years are considered (SCSN CATALOG, 1995): (a) 1980–1984, (b) 1985–1989, (c) 1990–1994. The solid straight-line in (a) to (c) is the Gutenberg–Richter relation (1) with $b = 1.05$ and $\dot{a} = 2.06 \times 10^5$ yr^{-1}, the best-fit to all data during 1980–1994. The larger number of earthquakes in 1987, 1992, and 1994 can be attributed to the aftershocks of the Whittier, Landers, and Northridge earthquakes, respectively. If aftershocks are excluded, the background seismicity in Southern California is nearly uniform in time.

(SCHOLZ, 1991). Further evidence for this comes from induced seismicity. Whenever the crust is loaded, whether in a tectonically active area or not, earthquakes are induced. Examples of loading include the filling of a reservoir behind a newly completed dam or the high-pressure injection of fluids in a deep well.

Since the eastern United States is a plate interior, the concept of rigid plates would preclude seismicity in the region. However, the plates act as stress guides. The forces that drive plate tectonics are applied at plate boundaries. Because the plates are essentially rigid, these forces are transmitted through their interiors. However, the plates have zones of weakness that will deform under these forces and earthquakes result. Thus, earthquakes occur within the interior of the surface plates of plate tectonics, although the occurrence frequencies are considerably lower than at plate boundaries.

As an example of intraplate seismicity we consider the New Madrid, Missouri, seismic zone. Three great earthquakes occurred here during the winter of 1811–1812. JOHNSTON and SCHWEIG (1996) suggest that two of these earthquakes had moment magnitudes $m = 8$. Based on both instrumental and historical records, JOHNSTON and NAVA (1985) have given the frequency-magnitude distribution for earthquakes in this region for the period 1816–1983. Their results are given in Figure 5. The data correlate well with the Gutenberg–Richter relation (1) taking $b = 0.90$ and $\dot{a} = 2.24 \times 10^3$ yr^{-1}.

Comparing Figures 3 and 5, the probability of having a moderate-sized earthquake in the New Madrid, Missourri area is about 1/60 the probability of having a similar magnitude earthquake in Southern California. Since the b-values for the two regions are about equal, this ratio is also applicable to other earthquake

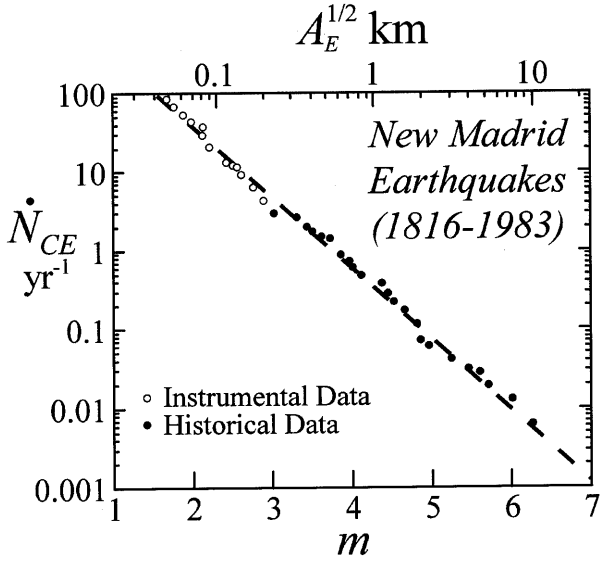

Figure 5
The cumulative number of earthquakes per year, $\dot{N}_{CE}$, occurring in the New Madrid, Missouri seismic zone (1816–1983) with magnitudes greater than m as a function of m. The open circles represent instrumental data and the solid circles historical data (JOHNSTON and NAVA, 1985). The straight dashed line is the Gutenberg–Richter relation (1) with $b = 0.90$ and $\dot{a} = 2.24 \times 10^3$ yr^{-1}.

magnitudes. This extrapolation is the basis of our global seismic hazards assessment. The results given in Figure 5 also provide further support for the hypothesis that the background seismicity in a region is independent of time. The instrumental data given in Figure 5 span a period of about 30 years and are in excellent agreement with the historical data that span 120 years.

The results given above support the use of the Gutenberg–Richter relation (1) to assess the global seismic hazard. We base our systematic global assessment of the seismic hazard on the epicenters of earthquakes with magnitudes $m \geq 4$, where the data were obtained from the NEIC Global Hypocenter Data Base (GHDB, 1989) for the period 1964–1995. We considered both a magnitude 5 cutoff and a magnitude 4 cutoff. The advantage of the magnitude 5 cutoff is that we could be certain that the database is globally complete for earthquakes $m \geq 5$ during this period (ENGDAHL *et al.*, 1998). The advantage of the magnitude 4 cutoff is that there are many more earthquakes on which to base our statistics. Since our primary goal is to provide the best seismic hazard assessment in populous regions, and since these regions generally have seismic networks that provide a complete catalog for $m \geq 4$ during this period, we have chosen this value for our cutoff. However, it should be emphasized that in some highly populated areas (for instance, some localities in the third world), the catalog is not complete down to magnitude 4 and the seismic hazard will be underestimated.

We include earthquakes from all depths in our analyses. On the downdip side of subduction zones this will lead to an overestimate of the seismic hazard. However, some relatively deep earthquakes can result in substantial damage and casualties.

In order to provide a map of the seismic hazard on a global basis, the surface of the earth was divided into $1° \times 1°$ regions and the number of earthquakes per year with magnitudes $m \geq 4$ in each region was determined. We defined the seismic intensity factor, I_4, as the number of magnitude $m \geq 4$ earthquakes that occurred in a given $1° \times 1°$ region per year, normalized by the cosine of the latitude. Normalization was due to areas changing with respect to changing latitude. For instance, take two $1° \times 1°$ regions, one at the equator and the other at 60° latitude. If the equator region has twice as many earthquakes as the one at 60°, then the density of earthquakes per area is equal.

The choice of $1° \times 1°$ regions may seem arbitrary. However, this is the minimum area over which consistent maps of free-air gravity can be made by averaging available measurements (TALWANI, 1970). Averaging of gravity observations is necessary because local free-air gravity measurements are very "noisy" due to uncompensated topography. When averages of measurements are made over $1° \times 1°$ areas this topographic noise is removed. In addition, our studies using different-sized areas for seismic averaging indicate that a $1° \times 1°$ area is optimal in terms of reducing noise and maximizing spatial resolution. There appears to be a tectonic variability on scales less than about 100 km that is reflected both in the uncompensated topography and the spatial variability of seismicity. FRANKEL (1995) found

that a Gaussian correlation length of 50 km was optimal for smoothing seismicity, similar to our choice.

A global map of the seismic intensity factor is given in Figure 6a. The boundaries of the tectonic plates are clearly defined. Seismicity is particularly intense in subduction zones (i.e., the ring of fire around the Pacific) as expected. A broad band of seismicity extends from Southern Europe to Southeast Asia, which is associated with continent–continent collision zones between the Eurasian plate and the African, Arabian, and Indian plates. The minimum value of the seismic intensity factor considered is $I_4 = 1/32$ yr^{-1}, one magnitude $m \geq 4$ earthquake in the 32-year period considered. The maximum value is about $I_4 = 40$ yr^{-1}, forty magnitude $m \geq 4$ earthquakes per year. The range of I_4 is over three orders of magnitude.

In Figure 7, two regional maps of the seismic intensity factor are given, the United States in Figure 7a and Europe in Figure 7b. For the United States, the intense seismicity on the boundary between the Pacific and North American plates (including the San Andreas Fault) is clearly illustrated. The distributed seismicity in the western United States is also shown. The most intense seismicity in the eastern United States is the New Madrid seismic zone (31 N, 90 W) as discussed above. For Europe, the Aegean region has particularly intense seismicity, however high levels of seismicity extend throughout the Mediterranean region.

The basis for using the seismic intensity factor, I_4, is illustrated in Figure 8. For five different values of I_4, the cumulative number of earthquakes per year in a $1° \times 1°$ area, $\dot{N}_{CE}$, with magnitudes greater than m is plotted as a function of m. The different lines are derived by using the Gutenberg–Richter relation (1) with $b = 0.9$, and calculating the constant $\dot{a}$ from $\log \dot{a} = 3.6 + \log I_4$ (TURCOTTE, 1999a). In Figure 8, given an area with $I_4 = 1$ yr^{-1}, an earthquake with $m \geq 6$ has a return period of 63 years ($\dot{N}_{CE} = 0.016$) and one with $m \geq 8$ has a return period of 4000 yrs ($\dot{N}_{CE} = 0.00025$).

It can be argued that the use of earthquakes with $m \geq 4$ for such a short period (37 years) would not represent the long-term seismic hazard. In order to address this concern, we used the NEIC Global Hypocenter Data Base (GHDB, 1989) to determine the largest earthquake occurring in each $1° \times 1°$ area for the period 1900–1997. These data are given in Figure 6b. Comparing Figures 6a and 6b, it is seen that there is a strong correlation between the value of the earthquake intensity factor, I_4, calculated using 32 years of data, and the largest earthquake to have occurred in each $1° \times 1°$ area, using 98 years of data.

Figure 6

(a) Global map of the seismic intensity factor I_4, the average annual number of earthquakes during the period 1964–1995 with magnitude $m \geq 4$ in each $1° \times 1°$ cell. (b) The maximum magnitude earthquake that occurred in each $1° \times 1°$ cell during the period 1900–1997. Data for both (a) and (b) are from the NEIC Global Hypocenter Data Base (GHDB, 1989).

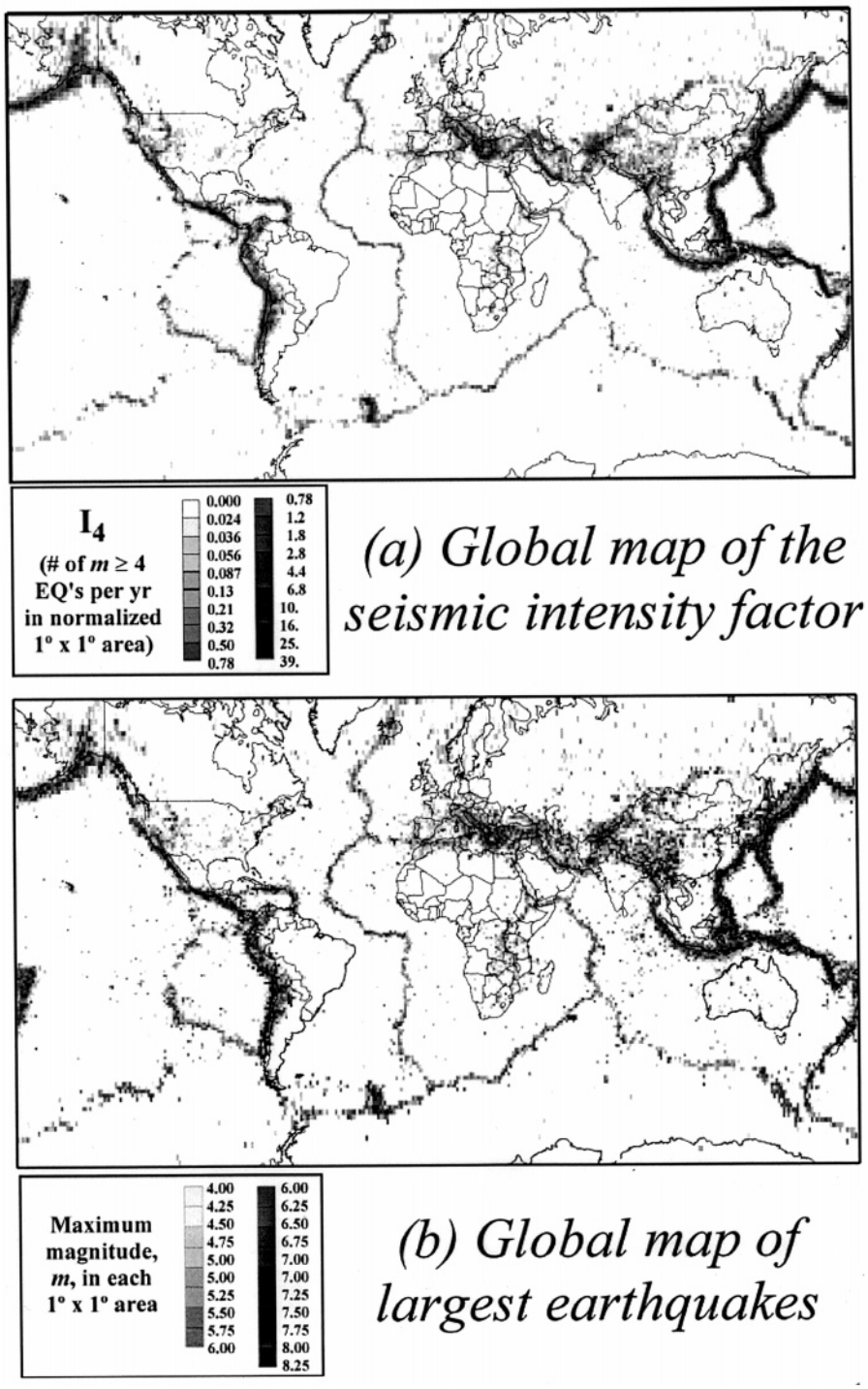
I4
(# of m ≥ 4 EQ's per yr in normalized 1° x 1° area)
0.000
0.024
0.036
0.056
0.087
0.13
0.21
0.32
0.50
0.78
0.78
1.2
1.8
2.8
4.4
6.8
10.
16.
25.
39.
(a) Global map of the seismic intensity factor
Maximum magnitude, m, in each 1° x 1° area
4.00
4.25
4.50
4.75
5.00
5.00
5.25
5.50
5.75
6.00
6.00
6.25
6.50
6.75
7.00
7.00
7.25
7.50
7.75
8.00
8.25
(b) Global map of largest earthquakes

Fig. 6.

A number of developed countries have prepared seismic hazard maps. In many cases, as discussed above, the local Gutenberg–Richter relation has been one of the inputs into the assessments. For the United States, the U.S. Geological Survey's

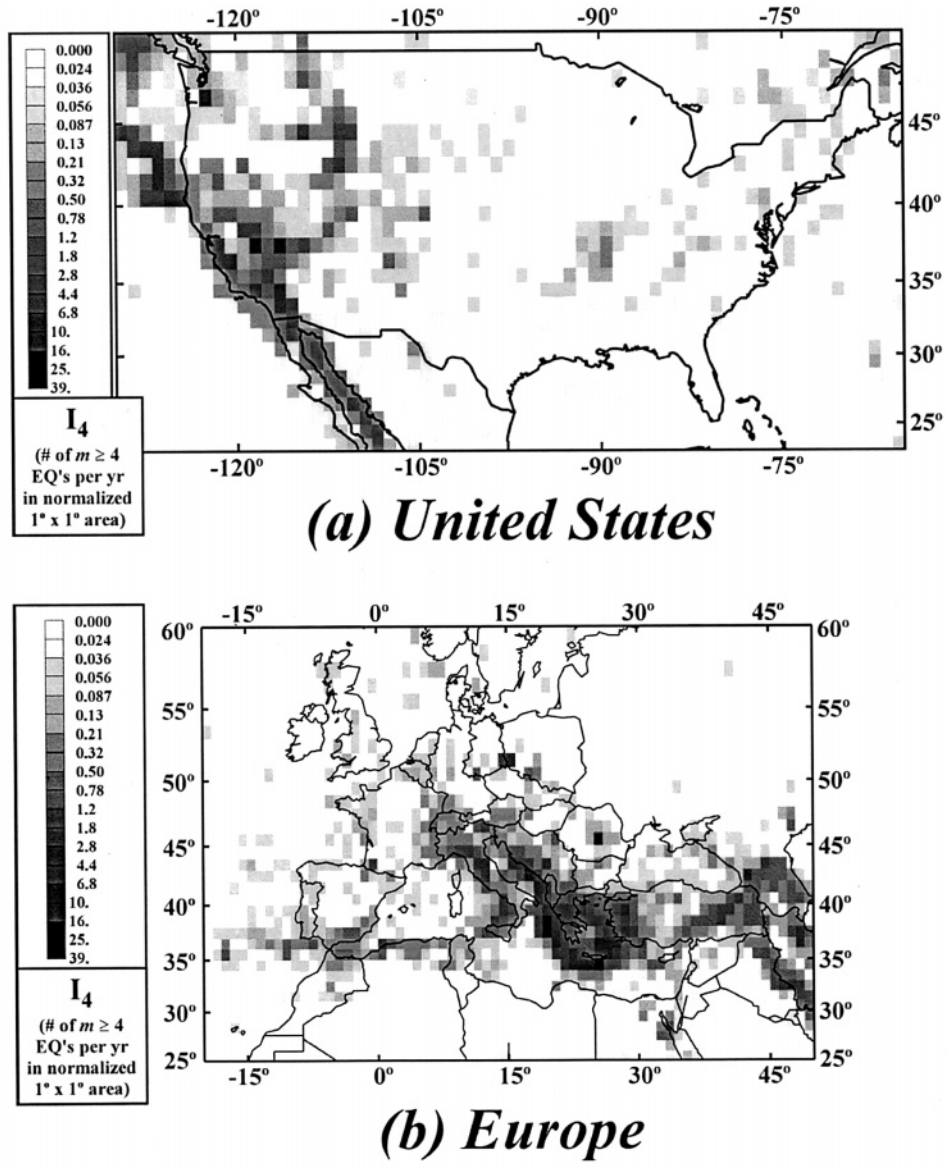

Figure 7

Regional maps of the seismic intensity factor I_4, the average annual number of earthquakes during 1964–1995 with magnitudes $m \geq 4$ in each normalized $1° \times 1°$ cell for (a) United States and (b) Europe. Data for both (a) and (b) are from the NEIC Global Hypocenter Data Base (GHDB, 1989).

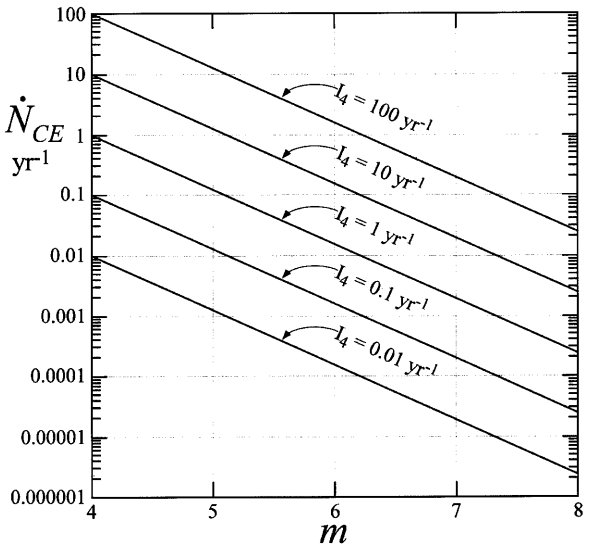

Figure 8
Similarity basis for extending the seismic intensity factor I_4 to higher earthquake magnitudes. See text for discussion.

June 1996 maps (FRANKEL *et al.*, 1996) are available on the internet. Seismic hazard maps generally give the probability of exceeding a specified peak ground acceleration during a specified time interval. The data used to formulate the maps include the historic seismicity discussed in this paper, maps of active faults, and levels of seismic attenuation. Taking 0.1 g as the reference acceleration, the return times for an earthquake that exceeds this value are the following (FRANKEL *et al.*, 1996): 23 years in Los Angeles, 27 years in San Francisco, 56 years in Seattle, 140 years in Salt Lake City, 150 years in Portland, 360 years in Memphis, 770 years in New York, 2900 years in Chicago, and 24,000 years in St. Paul.

We compare our approach for seismic hazard estimation to that used by the USGS by comparing probabilities in two regions: Southern California and the New Madrid seismic zone. We assume that the 23-year return time for Los Angeles is appropriate for Southern California and from Figure 3 find that the recurrence interval of 23 years ($\dot{N}_{CE} = 0.043$ yr^{-1}) corresponds to a magnitude $m \approx 7$ earthquake. From Figure 5, the recurrence time for a magnitude $m = 7$ earthquake in the New Madrid area is about 900 years ($\dot{N}_{CE} \approx 0.0011$ yr^{-1}); the USGS hazard assessment gives a return time, for 0.1 g acceleration, of 360 years for this region. The hazard assessment maps are reasonably consistent with the seismic intensity maps. The hazard assessment maps give a higher relative risk in aseismic zones because they include seismic attenuation that is less in aseismic zones. Comparisons for other regions can be made, based on the seismic intensity factors given in Figure 6a.

The primary advantage of our approach is that it is totally based on a generally accepted data set. There are no ambiguities with regard to the technique. This is not the case for other approaches to assessing seismic hazard, which combine geophysical and geological observations in arbitrary ways. Different studies give different weights to historical and paleo-seismic data, and to the presence of "active" faults. Considering the many uncertainties regarding fault depth, seismic attenuation, the available database, and the occurrence of an earthquake on a particular fault, we believe that the very simple approach we propose for assessing seismic hazard provides a reasonable approach based on the present level of knowledge. Another advantage of our approach is that it is applicable globally. Many countries with severe seismic hazards do not have the resources to carry out probabilistic seismic hazard assessments.

There are certainly objections to our approach. These include:

(1) The time interval used (in our case 32 yrs) is too short to establish a long-term rate of seismic activity. Strong earthquakes and their associated aftershocks will create local anomalies in the maps. We partially argue against this disadvantage, noting that with aftershocks removed, the background seismicity in Southern California (Fig. 4) on a year-to-year basis is essentially constant. In addition, there is close correspondence between the historical and recent instrumental data for New Madrid (Fig. 5). Observations favor the hypothesis that the rate of occurrence of smaller earthquakes in a region is only weakly dependent on time if the area is sufficiently large. If the smaller earthquakes correlated with the earthquake cycle, then they could be used for the temporal prediction of earthquakes. This is clearly not the case.

(2) The large "characteristic" earthquakes do not fall on an extrapolated Gutenberg–Richter curve. We have shown that this extrapolation is reasonably good for Southern California (Fig. 3). In addition, even if large earthquakes fall off the extrapolation, the hazard-assessment approach given above will be valuable for moderate-sized earthquakes.

(3) The extrapolation does not specify an upper limit to the expected earthquakes in a region. This is certainly true, but is a universal problem in seismic hazard assessment.

As discussed above, we are not the first to employ this technique. FRANKEL (1995) used a similar technique to contour values of 10^a ($\log N_{CE} = -bm + a$) for the eastern United States. His values of 10^a represent the number of earthquakes that occur in each 11 km $\times$ 11 km square grid in 60 years with $m > 0$. Note that in our nomenclature, $10^a = \tau \dot{a}$ where τ is the number of years considered, and $\dot{a}$ is the same as used in (1). His map (FRANKEL, 1995, Fig. 4) gives $10^a = 32$ for the New Madrid area, 8 for the Charleston area, 16 for eastern Tennessee, and 8 for New York City. Since 10^a is proportional to our I_4, these results can be compared to the results given in Figure 7a. Our results tend to give far greater variability between these regions.

3. Seismic Activation

We have discussed how small earthquakes can be used to quantify the hazard associated with large earthquakes. An important question is whether small earthquakes can be used to forecast the temporal occurrence of large earthquakes. As shown in Figure 4, the occurrence of the smallest earthquakes seems to have very little temporal dependence. However, there is accumulating evidence that there may be an activation of intermediate-sized earthquakes prior to a great earthquake. The occurrence of a relatively large number of intermediate-sized earthquakes in northern California prior to the 1906 San Francisco earthquake has been noted (SYKES and JAUMÉ, 1990). It has also been proposed that there is a power-law increase in seismicity prior to a major earthquake. This was first proposed by BUFE and VARNES (1993). They considered the cumulative amount of Benioff strain (square-root of seismic energy) in a specified region. They show that an accurate retrospective prediction of the Loma Prieta earthquake could be made, assuming a power-law temporal increase in Benioff strain prior to the earthquake.

Systematic increases in intermediate level seismicity before a large earthquake have been proposed by several authors (VARNES, 1989; BUFE *et al.*, 1994; KNOPOFF *et al.*, 1996; VARNES and BUFE, 1996; BREHM and BRAILE, 1998, 1999; JAUMÉ and SYKES, 1999). A systematic study of the optimal spatial region and magnitude range to obtain the power-law seismic activation has been carried out by BOWMAN *et al.* (1998). Four examples of their results are given in Figure 9. Clear increases in seismic activity prior to the Kern County, Loma Prieta, Landers, and Coalinga earthquakes are illustrated. In each case data for the cumulative Benioff strain ε is compared with the empirical relation (solid line)

$$\varepsilon[t] = \varepsilon_0 - B(t_0 - t)^s \tag{4}$$

where t is the time measured forward from the previous characteristic earthquake, t_0 is the time interval between characteristic earthquakes, ε_0 is the cumulative Benioff strain when the characteristic earthquake occurs, and B and s are positive constants used to fit the data. The comparison with the Kern County (July 21, 1952) data is made with $s = 0.30$, with Loma Prieta (October 18, 1989) $s = 0.28$, with Landers (June 28, 1992) $s = 0.18$, and with Coalinga (May 2, 1983) $s = 0.\ 18$.

BOWMAN *et al.* (1998) also found ξ the optimal radius (the correlation length) for the precursory activation. This optimal radius is given as a function of earthquake magnitude in Figure 10. The dependence on the square-root of rupture area is also shown. The radius over which activation occurs is about ten times the length of rupture, $\xi \approx 10A_E^{1/2}$. DOBROVOLSKY *et al.* (1979) and KEILIS-BOROK and KOSSOBOKOV (1990) reported earlier a similar scaling for the maximum distance between an earthquake and its precursors, using pattern recognition techniques.

The observations of seismic activation given above are consistent with results obtained from studies of cellular-automata slider-block models using a mean-field

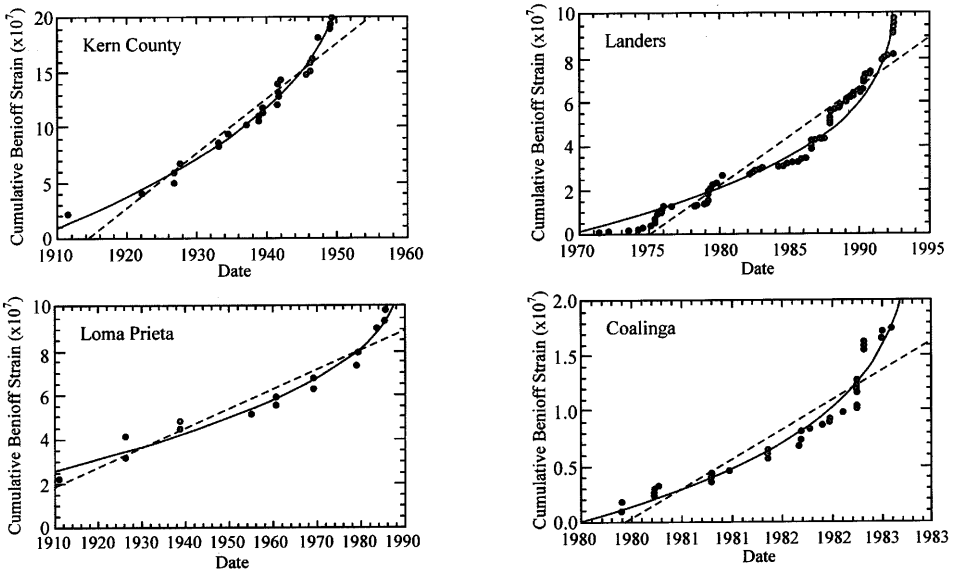

Figure 9
Power-law increases in the cumulative Benioff strains prior to four major earthquakes in California (BOWMAN *et al.*, 1998). Data points are cumulative Benioff strains $\varepsilon[t]$ prior to each earthquake. Clear increases in seismic activity prior to the 1952 Kern County, 1989 Loma Prieta, 1992 Landers, and 1983 Coalinga earthquakes are illustrated. In each of the four examples, the data have been correlated (solid lines) with the power-law relation given in (4). Dashed straight lines represent a best-fit constant rate of seismicity.

approach (RUNDLE *et al.*, 1996, 1997a,b, 1999; FISHER *et al.*, 1997). This approach involves concepts applied to equilibrium thermodynamics and the approach to a second-order phase transition through a spinoidal.

In the scaling associated with the approach to the critical point, the correlation length scales with the "rupture" length. This scaling follows directly from the spinoidal equation (RUNDLE *et al.*, 1997, Eq. 54). The details of this approach are given in RUNDLE *et al.* (2000). This is the scaling associated with the optimal activation length given in Figure 10. In addition, the rate of occurrence of events as the critical point is approached can be obtained (RUNDLE *et al.*, 2000, Eq. 16). This result can explain the rate of seismic activation given in (4).

4. Forecasting

Based on pattern recognition algorithms a number of intermediate-range earthquake prediction algorithms have been developed at the International Institute of Earthquake Prediction Theory and Mathematical Geophysics in Moscow (KEILIS-BOROK, 1990; KEILIS-BOROK and ROTWAIN, 1990; KEILIS-BOROK and KOS-

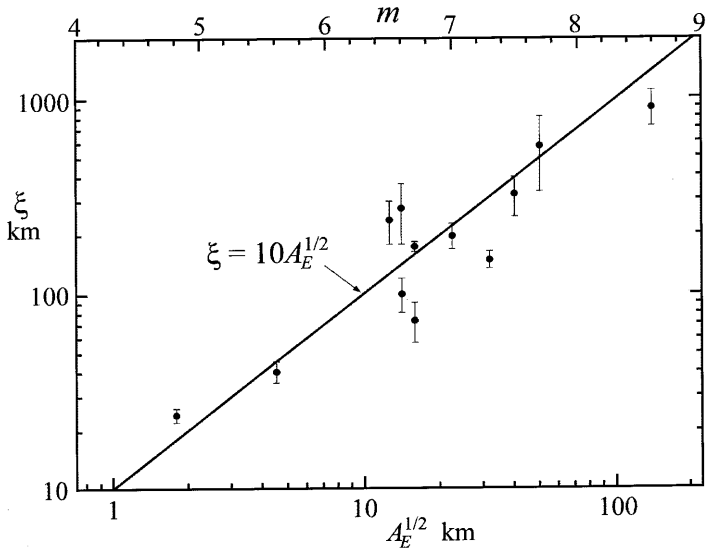

Figure 10
The optimum radius (correlation length) ξ for precursory seismic activation is given as a function of the square-root of the rupture area, $A_E^{1/2}$, and the magnitude, m, for twelve major earthquakes (Bowman *et al.*, 1998).

SOBOKOV, 1990). The pattern recognition includes seismic activation, quiescence (SCHREIDER, 1990), increases in the clustering of events, and changes in aftershock statistics (MOLCHAN *et al.*, 1990). The first algorithm, $M8$, was developed to make intermediate-term predictions of the largest earthquake ($m > 8$). This method utilizes overlapping circles of seismicity with diameters of 384, 560, 854, and 1333 km for earthquakes, with magnitudes 6.5, 7.0, 7.5, and 8.0, respectively. Within each circle four quantities are determined. The first three are measures of intermediate levels of seismicity and the fourth is a measure of aftershock activity.

The first quantity that must be specified is the lower magnitude cutoff $m_{\min}$ for earthquakes to be considered in the circle. Two magnitude cutoffs are considered for each circular region. The long-term number of earthquakes per year, $\dot{N}$, in the circle, with magnitudes greater than $m_{\min}$ is determined; $m_{\min 10}$ corresponds to $\dot{N} = 10$, and $m_{\min 20}$ corresponds to $\dot{N} = 20$. The first quantity $\dot{N}_1(t)$ is the number of earthquakes per year in the circle with magnitudes greater than $m_{\min 10}$ and $\dot{N}_2(t)$ is the number of earthquakes per year with magnitudes greater than $m_{\min 20}$ (both estimates over the preceding six-year window). The second quantity is the trend in activity $L_1 = \mathrm{d}\dot{N}_1/\mathrm{d}t$ and $L_2 = \mathrm{d}\dot{N}_2/\mathrm{d}t$ for running six-year windows. Clearly $\dot{N}(t)$ and $L(t)$ are strongly correlated. The third quantity, $Z_1(t)$ or $Z_2(t)$, is the ratio of the average linear dimension of rupture to the average separation between earthquakes for a running six-year window in a circle. The final measure is the number

of aftershocks in a specified magnitude range and time window following a main shock. This quantity $B(t)$ is a measure of aftershock activation.

Since $\dot{N}$, L, and Z are determined both for $\dot{N} = 10$ and 20 earthquakes per year there are seven time series to be considered. An earthquake alarm or time of increased probability (*TIP*) is issued if 6 of the 7 quantities, including B, exceed their average values by a specified value of 75% for B and 90% for the others. In order to issue an alarm, these conditions must be satisfied for two successive time periods and the alarm lasts for five years. Details of this algorithm have been given by KEILIS-BOROK (1996). Two examples of the application of this algorithm are given in Figure 11 (KEILIS-BOROK, 1996; KOSSOBOKOV *et al.*, 1999) for the 1989 Loma Prieta and the 1992 Landers earthquakes.

In order to refine the area in which a *TIP* is declared, the *MSc* (Mendocino scenario) algorithm was developed from studies of the seismicity prior to the Eureka (Cape Mendocino) earthquake (1980, $m = 7.2$). Using earthquakes with smaller magnitudes than in the $M8$ algorithm and utilizing transitions from excess seismicity to quiescence, this algorithm reduces the area over which a *TIP* is declared.

The algorithms described above were developed utilizing pattern recognition approaches. Although they have had demonstrated predictive successes (KOSSOBOKOV *et al.*, 1999; ROTWAIN and NOVIKOVA, 1999), their use remains quite controversial (ENEVA and BEN-ZION, 1997). The main difficulty is that, although success to failure ratios of predictions is quite high, the time and spatial windows of alarms are also quite high.

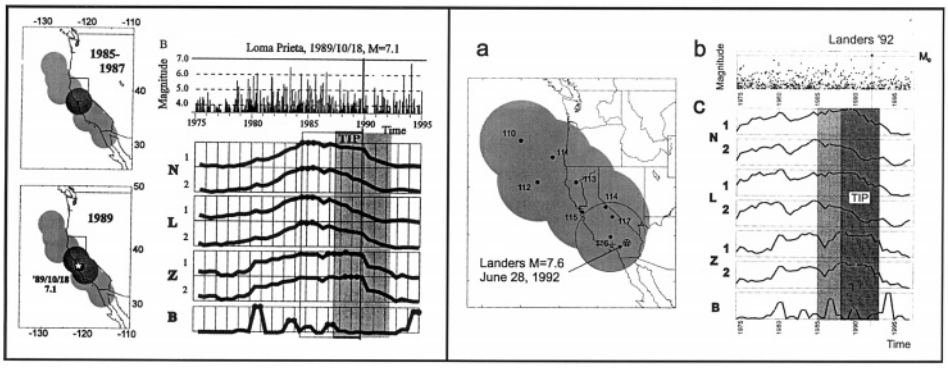

Figure 11

Applications of the $M8$ algorithm to (1) the $m = 7.1$ Loma Prieta earthquake (KEILIS-BOROK, 1996) and (2) the $m = 7.6$ Landers earthquake (KOSSOBOKOV *et al.*, 1999). For the Landers earthquake, part (a) of the right-half of the figure, the circular regions where "Times of Increased Probability" (*TIP*s) have been declared, are shown. In (b) the seismicity in the relevant region is shown. In (c) the values of the seven parameters $\dot{N}_1$, $\dot{N}_2$, L, L_1, L_2, Z_1, Z_2, and B are shown along with the time interval of the *TIP*.

There are clearly very strong similarities between the $M8$ algorithm and the seismic activation hypothesis. Consider the Loma Prieta earthquake, the intermediate-sized events that led to the $M8$ *TIP* illustrated in Figure 11 were the same events that generated the increase in Benioff strain illustrated in Figure 9. Both of these approaches are based on the concept that correlation lengths increase before major earthquakes (HARRIS, 1998).

5. Conclusions

We conclude that distributed seismicity is an example of both self-organized critical behavior and second-order critical-point behavior. Evidence for self-organizing critical behavior is the applicability under a wide variety of conditions of the Gutenberg–Richter frequency-magnitude relation. This is a power-law (fractal) scaling between the number of earthquakes and their rupture size. The number of small earthquakes in a region appears to be approximately constant in time. If this number varied with the temporal cycle of the characteristic earthquake in the region, then the number could be used for earthquake forecasting; this is clearly not the case. However, using Gutenberg–Richter scaling, the number of smaller earthquakes in a region can be extrapolated to assess the hazard of larger earthquakes in the region. Whether this can be done for the characteristic earthquake in the regional is controversial, however it certainly can be done for intermediate-sized earthquakes. Based on the extrapolation of the frequency of small earthquakes to larger earthquakes, we have given global maps of the seismic hazard. These utilize 32 years of instrumental seismic data, and averages are carried out over $1° \times 1°$ regions. These regions are selected because they remove the tectonic "grain."

It is widely accepted that the number of intermediate-sized earthquakes in a region increases prior to the characteristic earthquake for the region. This precursory activation has been shown to exhibit power-law scaling and to occur over a region about ten times larger than the rupture size of the characteristic earthquake. This precursory activation is the primary basis for the use of the $M8$ algorithm that has been developed empirically for earthquake forecasting.

Both the Gutenberg–Richter scaling and the precursory activation are consistent with the application of condensed-matter theory to regional seismicity. The scaling of small earthquakes in a region is equivalent to the thermal fluctuations in solids, liquids, and gases. This behavior falls under the general class of phenomena that exhibit self-organized critical behavior. Examples include the sandpile, slider-block, and forest-fire models. These models are characterized by a fractal. frequency-area distribution of avalanches; model sand slides, slip events, and forest fires. These models can be explained in terms of an inverse-cascade involving the coalescence of metastable clusters.

The characteristic earthquake appears to behave as a second-order phase change. As the phase change is approached the scale of the region over which correlated activity occurs (the correlation length) increases. In terms of earthquakes, this correlated region is the region of precursory activation. Analyses of the spinoidal behavior associated with second-order phase transitions predict the power-law increase in seismic activity prior to a characteristic earthquake.

Acknowledgements

The authors wish to acknowledge many useful discussions with Gleb Morein, John Rundle and Charlie Sammis. This manuscript benefited significantly from the detailed and thorough comments of two anonymous reviewers. The authors received support from NSF grant EAR 9804859.

REFERENCES

AKI, K., *A probabilistic synthesis of precursory phenomena*. In *Earthquake Prediction* (eds. Simpson, D. W., and Richards, P. G.) (American Geophysical Union, Washington, D.C. 1981) pp. 566–574.

BAK, P., TANG, C., and WIESENFELD, K. (1988), *Self-organized Criticality*, Phys. Rev. *A38*, 364–374.

BAK, P., and TANG, C. J. (1989), *Earthquakes as a Self-organized Critical Phenomenon*, J. Geophys. Res. *94*, 15,635–15,637.

BERNREUTER, D. L., SAVY, J. B., MENSING, R. W., and CHEN, J. C., *Seismic Hazard Characterization of 69 Nuclear Plant Sites East of the Rocky Mountains* (U.S. Nuclear Regulatory Commission NUREG/CR-5250 UCID-21517, 8 volumes, Washington, D.C. 1989).

BOWMAN, D. D., OUILLON, G., SAMMIS, C. G., SORNETTE, A., and SORNETTE, D. (1998), *An Observational Test of the Critical Earthquake Concept*, J. Geophys. Res. *103*, 24,359–24,372.

BREHM, D. J., and BRAILE, L. W. (1998), *Intermediate-term Earthquake Prediction Using Precursory Events in the New Madrid Seismic Zone*, Bull. Seismol. Soc. Am. *88*, 564–580.

BREHM, D. J., and BRAILE, L. W. (1999), *Intermediate-term Earthquake Prediction Using the Modified Time-to-failure Method in Southern California*, Bull. Seismol. Soc. Am. *89*, 275–293.

BROWN, S. R., SCHOLZ, C. H., and RUNDLE, J. B. (1991), *A Simplified Spring-block Model of Earthquakes*, Geophys. Res. Lett. *18*, 215–218.

BUFE, C. G., and VARNES, D. J. (1993), *Predictive Modeling of the Seismic Cycle of the Greater San Francisco Bay Region*, J. Geophys. Res. *98*, 9871–9883.

BUFE, C. G., NISHENKO, S. P., and VARNES, D. J. (1994), *Seismicity Trends and Potential for Large Earthquakes in the Alaska-Aleutian Region*, Pure appl. geophys. *142*, 83–99.

BURRIDGE, R., and KNOPOFF, L. (1967), *Model and Theoretical Seismicity*, Bull. Seismol. Soc. Am. *57*, 341–371.

CARLSON, J. M., and LANGER, J. S. (1989), *Mechanical Model of an Earthquake Fault*, Phys. Rev. *A40*, 6470–6484.

CARLSON, J. M., LANGER, J. S., and SHAW, B. E. (1994), *Dynamics of Earthquake Faults*, Rev. Mod. Phys. *66*, 657–670.

CORNELL, A. C. (1968), *Engineering Seismic Risk Analysis*, Bull. Seismol. Soc. Am. *58*, 1583–1606.

DAVISON, F., and SCHOLZ, C. H. (1985), *Frequency-moment Distribution of Earthquakes in the Aleutian Arc: A Test of the Characteristic Earthquake Model*, Bull. Seismol. Soc. Am. *75*, 1349–1362.

DOBROVOLSKY, I. R., ZUBKOV, S. I., and MIACHKIN, V. I. (1979), *Estimation of the Size of Earthquake Preparation Zones*, Pure appl. geophys. *117*, 1025–1044.

ENEVA, M., and BEN-ZION, Y. (1997), *Techniques and Parameters to Analyze Seismicity Patterns Associated with Large Earthquakes*, J. Geophys. Res. *102*, 17,785–17,795.

ENGDAHL, E. R., VAN DER HILST, R., and BULAND, R. (1998), *Global Teleseismic Earthquake Relocation with Improved Travel Times and Procedures for Depth Determination*, Bull. Seismol. Soc. Am. *88*, 722–743.

FISHER, D. S., DAHMEN, K., RAMANATHAN, S., and BEN-ZION, Y. (1997), *Statistics of Earthquakes in Simple Models of Heterogeneous Faults*, Phys. Rev. Lett. *78*, 4885–4888.

FRANKEL, A. F. (1995), *Mapping Seismic Hazard in the Central and Eastern United States*, Seis. Res. Lett. *60* (4), 8–21.

FRANKEL, A. F., MUELLER, C., BARNHARD, T., PERKINS, D., LEYENDECKER, E. V., DICKMAN, N., HANSON, S., and HOPPER, M., *National Seismic Hazard Maps* (USGS Open-File Report 1996) pp. 96–532.

FROHLICH, C., and DAVIS, S.D. (1993), *Teleseismic b Values; or*, *Much Ado About 1.0*, J. Geophys. Res. *98*, 631–644.

GELLER, R. J., JACKSON, D. D., KAGAN, Y. Y., and MULARGIA, F. (1997), *Earthquakes Cannot Be Predicted*, Science *275*, 1616–1617.

GHDB (1989), *Global Hypocenter Data Base (GHDB)*, CD ROM (NEIC/USGS, Denver, Colorado, 1989) and its updates through 1997.

GUTENBERG, B., and RICHTER, C. F., *Seismicity of the Earth and Associated Phenomenon*, *2nd ed* (Princeton University Press, Princeton 1954).

HARRIS, R. A. (1998), *Forecasts of the 1989 Loma Prieta*, *California*, *Earthquake*, Bull. Seismol. Soc. Am. *88*, 898–916.

HUANG, J., and TURCOTTE, D. L. (1990), *Are Earthquakes an Example of Deterministic Chaos?*, Geophys. Res. Lett. *17*, 223–226.

HUANG, J., NARKOUNSKAIA, G., and TURCOTTE, D. L. (1992), *A Cellular-automata*, *Slider-block Model for Earthquakes II. Demonstration of Self-organized Criticality for a 2-D System*, Geophys. J. Int. *111*, 259–269.

JAUMÉ, S. C., and SYKES, L. R. (1999), *Evolving Towards a Critical Point: A Review of Accelerating Seismic Moment/Energy Release Prior to Large and Great Earthquakes*, Pure appl. geophys. *155*, 279–305.

JOHNSTON, A. C., and NAVA, S. J. (1985), *Recurrence Rates and Probability Estimates for the New Madrid Seismic Zone*, J. Geophys. Res. *90*, 6737–6753.

JOHNSTON, A. C., and SCHWEIG, E. S. (1996), *The Enigma of the New Madrid Earthquakes of 1811–1812*, An. Rev. Earth Planet. Sci. *24*, 339–384.

KADANOFF, L. P., NAGEL, S. R., WU, L., and ZHOU, S. M. (1989), *Scaling and Universality in Avalanches*, Phys. Rev. *A39*, 6524–6533.

KEILIS-BOROK, V. I. (1990), *The Lithosphere of the Earth as a Nonlinear System with Implications for Earthquake Prediction*, Rev. Geophys. *28*, 19–34.

KEILIS-BOROK, V. I. (1996), *Intermediate-term Earthquake Prediction*, Proc. Natl. Acad. Sci. *93*, 3748–3755.

KEILIS-BOROK, V. I., and KOSSOBOKOV, V. G. (1990), *Premonitory Activation of Earthquake Flow*. *Algorithm M8*, Phys. Earth Planet. Int. *61*, 73–83.

KEILIS-BOROK, V. I., and ROTWAIN, I. M. (1990), *Diagnosis of Time of Increased Probability of Strong Earthquakes in Different Regions of the World: Algorithm CN*, Phys. Earth Planet. Int. *61*, 57–72.

KNOPOFF, L., LEVSHINA, T., KEILIS-BOROK, V. I., and MATTONI, C. (1996), *Increased Long-range Intermediate-magnitude Earthquake Activity Prior to Strong Earthquakes in California*, J. Geophys. Res. *101*, 5779–5796.

KOSSOBOKOV, V. G., ROMASHKOVA, L. L., KEILIS-BOROK, V. I., and HEALY, J. H. (1999), *Testing Earthquake Prediction Algorithms: Statistically Significant Advance Prediction of the Largest Earthquakes in the Circum-Pacific*, *1992–1997*, Phys. Earth Planet. Int. *111*, 187–196.

LAY, T., and WALLACE, T. C., *Modern Global Seismology* (Academic Press, San Diego 1995).

LORENZ, E. N. (1963), *Deterministic Nonperiodic Flow*, J. Atmos. Sci. *20*, 130–141.

MALAMUD, B. D., MOREIN, G., and TURCOTTE, D. L. (1998), *Forest Fires: An Example of Self-organized Critical Behavior*, Science *281*, 1840–1842.

MAY, R. M. (1976), *Simple Mathematical Models with Very Complicated Dynamics*, Nature *261*, 459–467.

MOLCHAN, G. M., DMITRIEVA, O. E., ROTWAIN, I. M., and DEWEY, J. (1990), *Statistical Analysis of the Results of Earthquake Prediction, Based on Bursts of Aftershocks*, Phys. Earth Planet. Int. *61*, 128–139.

NAKANISHI, H. (1991), *Statistical Properties of the Cellular Automata Model for Earthquakes*, Phys. Rev. *A43*, 6613–6621.

OTSUKA, M. (1972), *A Simulation of Earthquake Occurrence*, Phys. Earth Planet. Int. *6*, 311–315.

PACHECO, J., SCHOLZ, C. H., and SYKES, L. R. (1992), *Changes in Frequency-size Relationship from Small to Large Earthquakes*, Nature *355*, 71–73.

PELLETIER, J. D., MALAMUD, B. D., BLODGETT, T., and TURCOTTE, D. L. (1997), *Scale-invariance of Soil Moisture Variability and its Implications for the Frequency-size Distribution of Landslides*, Eng. Geol. *48*, 255–268.

ROTWAIN, I., and NOVIKOVA, O. (1999), *Performance of the Earthquake Prediction Algorithm CN in 22 Regions of the World*, Phys. Earth Planet. Int. *111*, 207–213.

RUNDLE, J. B., GROSS, S., KLEIN, W., FERGUSON, C., and TURCOTTE, D. L. (1997a), *The Statistical Mechanics of Earthquakes*, Tectonophys. *277*, 147–164.

RUNDLE, J. B., KLEIN, W., and GROSS, S. (1996), *Dynamics of a Traveling Density Wave Model for Earthquakes*, Phys. Rev. Lett. *76*, 4285–4288.

RUNDLE, J. B., KLEIN, W., and GROSS, S. (1999), *Physical Basis for Statistical Patterns in Complex Earthquake Populations: Models, Predictions, and Tests*, Pure appl. geophys. *155*, 575–607.

RUNDLE, J. B., KLEIN, W., GROSS, S., and FERGUSON, C. D. (1997b), *The Traveling Density Wave Model for Earthquakes and Driven Threshold Systems*, Phys. Rev. *E56*, 293–307.

RUNDLE, J. B., KLEIN, W., TURCOTTE, D. L., and MALAMUD, B. D. (2000), *Precursory Seismic Activation and Critical Point Phenomena*, Pure appl. geophys. *157*, 2165–2182.

SCHOLZ, C. H., in *Spontaneous Formation of Space Time Structure and Criticality* (eds. Riste, T., and Sherrington, D.) (Kluwer, Amsterdam 1991) pp. 41–56.

SCHOLZ, C. H. (1997), *Size Distributions for Large and Small Earthquakes*, Bull. Seismol. Soc. Am. *87*, 1074–1077.

SCHREIDER, S. (1990), *Formal Definition of Premonitory Seismic Quiescence*, Phys. Earth Planet. Int. *61*, 113–127.

SCSN CATALOG. *Southern California Seismographic Network Catalog in Electronic Format at the Southern California Earthquake Center (SCEC) Data Center* (California Institute of Technology, Pasadena, California 1995).

SIEH, K. E. (1978), *Slip Along the San Andreas Fault Associated with the Great 1857 Earthquake*, Bull. Seismol. Soc. Am. *68*, 1421–1448.

SIEH, K. E., STUIVER, M., and BRILLINGER, D. (1989), *A More Precise Chronology of Earthquakes Produced by the San Andreas Fault in Southern California*, J. Geophys. Res. *94*, 603–623.

SYKES, L. R., and JAUMÉ, S. C. (1990), *Seismic Activity on Neighboring Faults as a Long-term Precursor to Large Earthquakes in the San Francisco Bay Area*, Nature *348*, 595–599.

TALWANI, M., *Gravity*. In *The Sea* (ed. Maxwell, A. E.), vol. 4, part I (Wiley-Interscience, New York 1970) pp. 251–297.

TURCOTTE, D. L. (1989), *A Fractal Approach to Probabilistic Seismic Hazard Assessment*, Tectonophys. *167*, 171–177.

TURCOTTE, D. L. (1991), *Earthquake Prediction*, An. Rev. Earth Planet. Sci. *19*, 263–281.

TURCOTTE, D. L., *Fractals and Chaos in Geology and Geophysics, 2nd ed* (Cambridge University Press, Cambridge 1997).

TURCOTTE, D. L. (1999a), *Seismicity and Self-organized Criticality*, Phys. Earth Planet. Int. *111*, 275–293.

TURCOTTE, D. L. (1999b), *Self-organized Criticality*, Rep. Prog. Phys. *62*, 1377–1429.

TURCOTTE, D. L., MALAMUD, B. D., MOREIN, G., and NEWMAN, W. I. (1999), *An Inverse-cascade Model for Self-organized Critical Behavior*, Physica *A268*, 629–643.

VARNES, D. J. (1989), *Predicting Earthquakes by Analyzing Accelerating Precursory Seismic Activity*, Pure appl. geophys. *130*, 661–686.

VARNES, D. J., and BUFE, C. G. (1996), *The Cyclic and Fractal Seismic Series Preceding an m_b 4.8 Earthquake on 1980 February 14 near the Virgin Islands*, Geophys. J. Int. *124*, 149–158.

(Received August 12, 1999, revised May 3, 2000, accepted May 5, 2000)